Topography optimization for enhancing Microalgal growth in raceway ponds

Olivier Bernard[1,2], Liu-Di Lu[1,3,4], Jacques Sainte-Marie[3,4],
Julien Salomon[3,4]

[1] *INRIA Sophia Antipolis Méditerranée, BIOCORE Project-Team, Université Nice Côte d'Azur, 2004, Route des Lucioles - BP 93, 06902 Sophia-Antipolis Cedex, France*

[2] *Sorbonne Université, INSU-CNRS, Laboratoire d'Océanographie de Villefranche, 181 Chemin du Lazaret, 06230 Villefranche-sur-mer, France*

[3] *INRIA Paris, ANGE Project-Team, 75589 Paris Cedex 12, France*

[4] *Sorbonne Université, CNRS, Laboratoire Jacques-Louis Lions, 75005 Paris, France*

Abstract

We consider a coupled hydrodynamical-biological model describing growth in a microalgal raceway pond cultivation. More precisely, our approach combines a biological model (based on the Han model) and Saint-Venant systems that model the fluid into the raceway pond. Here we focus on the laminar fraction of the fluid, far from the paddle wheel, considering different topographies to enhance the microalgal growth rate. We present an optimization problem derived from the Pontryagin Maximum Principle dealing with the topography to maximize the biomass production over one lap or multiple laps with a paddle wheel. On the contrary to a widespread belief in the microalgae field, the results show that a flat topography is optimal in a periodic regime. In other frameworks, non-trivial topographies can be obtained. We present some of them, e.g., when the mixing device is also taken into account in the model.

Keyword: Optimal control, PMP, shape optimization, Han model, Saint-Venant system, Microalgal raceway

1 Introduction

Numerical design of microalgae production technologies has been for decades a source of many interesting challenges not only in engineering but also in the area of scientific computing [14, 24, 35, 21]. The potential of these emerging photosynthetic organisms finds interests for the cosmetics, pharmaceutical fields, feed, food and - in the longer term - green chemistry and energy applications [34].

1

Outdoor production is mainly carried out in open bioreactors with a raceway shape. Algae grow while exposed to solar radiation in such circular basins, where the water is set in motion by a paddle wheel. This mixing device homogenizes the medium for ensuring an equidistribution of the nutrients and guarantees that each cell will have regularly access to light [10, 13]. The algae are periodically harvested, and their concentration is maintained around an optimal value [28, 31]. Light penetration is strongly reduced by the algal biomass, and less than 1% [6] of the incident light reaches the reactor bottom. For larger biomass, the light extinction is so high that a large fraction of the population evolves in the dark and does not grow anymore. At low biomass density, a fraction of the solar light is not used by the algae and the productivity is suboptimal. Theoretical works have determined the optimal biomass for maximizing productivity [23, 17].

Here, we consider another approach which consists in improving the photoproduction process by controlling the cell trajectories in the light field. We starts from the observation that algal raceway ponds are dynamical systems conjugating a physical aspect - the hydrodynamical behaviour of the fluid transporting the algae culture, and a biological aspect - the light harvesting by the chlorophyll complexes in the cells [1, 29, 30]. We then study the effect of the topography (or the bathymetry) on growth to optimize the light received by the microalgae. Modelling the corresponding system is challenging since it involves the free-surface incompressible Navier-Stokes system [8, 11, 33, 27]. The complexity of this model generally prevents obtaining explicit formulas and large computational resources are required to carry out simulations.

Several experimental campaigns [25, 32] have shown that in the raceway straight sections, there are no features that disturb the flow (and this was further confirmed by CFD modelling [19, 20]. Therefore, in these systems, despite turbulent dispersion, mixing is relatively poor. The mixing is mainly induced locally by the paddle wheel, and in a lesser extend by the bends. The more recent study of [20] confirms this finding, showing that most of the turbulence is generated in the neighborhood of the paddle wheel and close to the surface.

We therefore focus on the main part of the raceway, outside the paddle wheel area, and we assume a laminar flux. We study how to enhance productivity in this part by modifying the bottom topography. This enables us to discuss a common belief that some specific topographies can bring more light to the algae (at the lower part of the raceway), since cells get closer to the surface when reaching the peak of these topographies.

Let us detail our approach. We first introduce a coupled model to represent the growth of algae in a raceway pond, accounting for the light that they receive due to advection in the fluid field. This model is obtained by combining the Han photosynthesis equations with a hydrodynamic law based on the Saint-Venant system. This first step enables us to formulate an optimization problem where the raceway topography is designed to maximize the productivity. Here, we use an adjoint-based optimization scheme to includes the constraints associated with the Saint-Venant regime. We then prove that the flat topography is optimal for productivity in a periodic case, when focusing on the fraction of the raceway with laminar regime. However, non-trivial topographies can be ob-

2

tained in other contexts, e.g., when the periodic assumption is removed or when the mixing device is accounted for in conjunction with the bottom topography. Final simulations considering a combination of turbulence induced mixing and non flat topographies can slightly increase biomass production. However, enhancing turbulence by mixing will more significantly increase productivity and will definitely be the most efficient approach [4, 5], even if more energy will be dissipated by turbulence.

The outline of the paper is as follows. In Section 2, we present the biological and hydrodynamical models underlying our coupled system. In Section 3, we describe the optimization problem and a corresponding numerical optimization procedure. Section 4 is devoted to the numerical results obtained with our approach. We conclude then with some perspectives opened by this work.

2 Hydrodynamic and biological models

Our approach is based on a coupling between the hydrodynamic behavior of the particles and the evolution of the photosystems driven by the light intensity they receive when traveling across the raceway pond.

2.1 Hydrodynamical model and Lagrangian trajectories

The Saint-Venant equations are one of the most popular model for describing geophysical flows, which is derived from the free surface incompressible Navier-Stokes equations (see for instance [15]). In this paper, we focus on the smooth steady state solutions of the Saint-Venant equations in a laminar regime. Such steady states are governed by the following partial differential equations:

$$\partial_x(hu) = 0, \quad \partial_x(hu^2 + g\frac{h^2}{2}) = -gh\partial_x z_b, \tag{1}$$

where h is the water depth, u is the horizontal averaged velocity of the water, the constant g stands for the gravitational acceleration and z_b defines the topography. The free surface η is given by $\eta = h + z_b$ and the averaged discharge $Q = hu$. This system is presented in Fig. 1. The z (resp. x) axis represents the vertical (resp. horizontal) direction and I_s is the light intensity at the free surface (assumed to be constant).

Integrating equation on the left of (1), we get

$$hu = Q_0, \tag{2}$$

for a fixed positive constant Q_0, which implies a constant discharge in space. Then equation on the right of (1) can be rewritten by

$$hu\partial_x u + h\partial_x gh + h\partial_x gz_b = 0. \tag{3}$$

Let us assume that h is strictly positive. Dividing (3) by h and using (2) to eliminate u, we get $\partial_x\left(\frac{Q_0^2}{2h^2} + g(h + z_b)\right) = 0$. Now consider two fixed constants
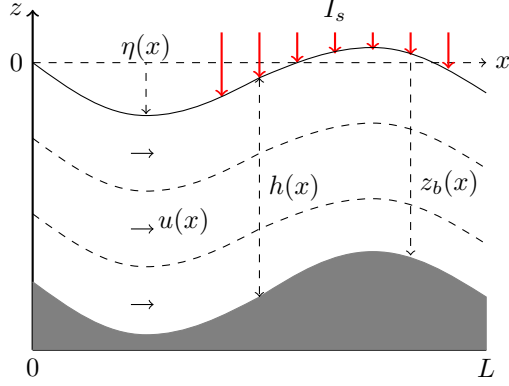
3

Figure 1: Representation of the hydrodynamic model.

$h(0), z_b(0) \in \mathbb{R}$, for all $x \in [0, L]$, we obtain $\frac{Q_0^2}{2h^2} + g(h + z_b) = \frac{Q_0^2}{2h^2(0)} + g(h(0) + z_b(0)) =: M_0$, meaning that the topography z_b satisfies

$$z_b = \frac{M_0}{g} - \frac{Q_0^2}{2gh^2} - h. \tag{4}$$

Remark 2.1. *Define the Froude number for the steady state by $Fr = u/\sqrt{gh}$. The situation $Fr < 1$ corresponds to the subcritical case (i.e. the flow regime is fluvial) while $Fr > 1$ is to the supercritical case (i.e. the flow regime is torrential). In particular, the threshold value of h for $Fr = 1$ is given by $h_c := (\frac{Q_0^2}{g})^{\frac{1}{3}}$.*

Because of (4), h is the solution of a third order polynomial equation. Given a smooth topography z_b, if $h_c + z_b + \frac{Q_0^2}{2gh_c^2} - \frac{M_0}{g} < 0$. there exists a unique positive smooth solution of (4) which satisfies the subcritical flow condition (see [26, Lemma 1]). Let $z(t)$ be the depth of a particle at time t in the raceway pond. We first determine the Lagrangian trajectory of an algal cell that starts at a given position $z(0)$ at time 0. From the incompressibility of the flow, we have $\nabla \cdot \underline{u} = 0$ with $\underline{u} = (u(x), w(x, z))$. Here, $w(x, z)$ is the vertical velocity. The incompressibility implies that $\partial_x u + \partial_z w = 0$. Integrating the latter from z_b to z gives:

$$
\begin{aligned}
0 &= \int_{z_b}^{z} \big(\partial_x u(x) + \partial_z w(x, z) \big) \mathrm{d}z \\
&= \partial_x \big((z - z_b) u(x) \big) + w(x, z) - w(x, z_b) \\
&= (z - z_b) \partial_x u(x) - u(x) \partial_x z_b + w(x, z),
\end{aligned}
$$

where we have used the kinematic condition at the bottom (i.e. $w(x, z_b) =$

$u(x)\partial_x z_b)$. It follows from (4) that

$$w(x, z) = (\frac{M_0}{g} - \frac{3u^2(x)}{2g} - z)u'(x). \tag{5}$$

The Lagrangian trajectory is characterized by

$$\begin{pmatrix} \dot{x}(t) \\ \dot{z}(t) \end{pmatrix} = \begin{pmatrix} u(x(t)) \\ w(x(t), z(t)) \end{pmatrix}. \tag{6}$$

Remark 2.2. *The geometry of the raceway pond with small dissipation and shear effects (reduced wall friction and viscosity) justifies a laminar flow modelled by a shallow water model, such as the Saint-Venant system. This regime also minimizes the mixing energy, hence is favoured at industrial scale.*

A higher mixing energy would lead to a turbulent regime. A possible way to enrich the representation of the Lagrangian trajectories in this case would consists in adding a Brownian motion to the definition (6). *However, getting time-free expressions of the trajectories (as in Equations* (7) *and* (11)*) in this case is much more challenging so that such a strategy would require a large set of simulations together with an averaging strategy.*

The previous expression of the Lagrangian trajectory (6) is a general formulation which still holds when we change the hydrodynamical model. Based on the special form of the chosen Saint-Venant system, we can find a simpler formulation of the Lagrangian trajectory. More precisely, we denote by $z(x)$ the depth of a particle at the position x. From (5) and (6), we get

$$z' := \frac{\dot{z}}{\dot{x}} = (\frac{M_0}{g} - \frac{3u^2}{2g} - z)\frac{u'}{u}. \tag{7}$$

Note that from (2) and (4), we have $\eta = h + z_b = \frac{M_0}{g} - \frac{u^2}{2g}$, which implies $\eta' = -uu'/g$. Multiplying (7) both sides by u and using the formulation of η, η' gives $z'u + zu' = (\eta - \frac{u^2}{g})u' = \eta u' + \eta' u$, which implies that $(u(z - \eta))' = 0$. Using (2), we then obtain

$$\eta(x) - z(x) = \frac{h(x)}{h(0)}(\eta(0) - z(0)). \tag{8}$$

This equation shows that given the data $h(0), \eta(0), z(0)$, the distance between a point in a trajectory and the surface depends only on $h(x)$. We exploit this property of the model in section 3.

Remark 2.3. *Since Q_0 is chosen to be positive, h is necessarily positive. Moreover, if $z(0)$ belongs to $[z_b(0), \eta(0)]$, then $z(x)$ belongs to $[z_b(x), \eta(x)]$. In particular, choosing $z(0) = z_b(0)$ in* (8) *and using* (2) *gives $z(x) = z_b(x)$. In the same way, we find that $z(x) = \eta(x)$ when $z(0) = \eta(0)$.*

2.2 Modeling the photosystems dynamics

We consider the Han model [18] which describes the dynamics of the reaction centers. These subunits of the photosynthetic process harvest photons and transfer their energy to the cell to fix CO_2. In this compartmental model, the photosystems can be described by three different states: open and ready to harvest a photon (A), closed while processing the absorbed photon energy (B), or inhibited if several photons have been absorbed simultaneously (C). The relation of these three states are schematically presented in Fig. 2.
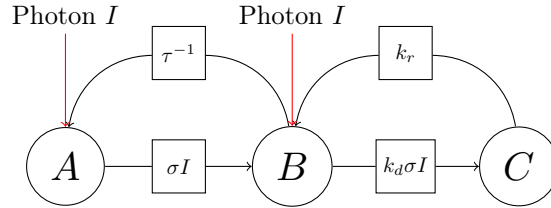

Figure 2: Scheme of the Han model, representing the probability of state transition, as a function of the photon flux density.

Their evolution satisfy the following dynamical system

$$\begin{cases} \dot{A} = -\sigma I A + \frac{B}{\tau}, \\ \dot{B} = \sigma I A - \frac{B}{\tau} + k_r C - k_d \sigma I B, \\ \dot{C} = -k_r C + k_d \sigma I B. \end{cases} \tag{9}$$

Here I is the photon flux density, a continuous time-varying signal. A, B and C are the relative frequencies of the three possible states with $A + B + C = 1$, so that (9) can be reduced to a system in dimension 2 by eliminating B. The other parameters are σ, that stands for the specific photon absorption, τ which is the turnover rate, k_r which represents the photosystem repair rate and k_d which is the damage rate. The dynamics of the open state A can be shown to be much faster than the dynamics of the photoinhibition state C. A slow-fast approximation by using singular perturbation theory (as shown in [21]) leads to the simplification of the dynamics driven by the slow dynamics of C:

$$\dot{C} = -\alpha(I)C + \beta(I), \tag{10}$$

where $\alpha(I) = \beta(I) + k_r$ with $\beta(I) = k_d \tau \frac{(\sigma I)^2}{\tau \sigma I + 1}$. Repeating the reasoning done to get (7) with (10) and (2), we find a time-free reformulation, namely

$$C' := \frac{\dot{C}}{\dot{x}} = \frac{-\alpha(I)C + \beta(I)}{Q_0} h, \tag{11}$$

where all the functions on the right-hand side only depend on the spatial variable x. Finally, the net growth rate is defined by balancing photosynthesis and

respiration, which gives

$$\mu(C, I) := -\gamma(I)C + \zeta(I), \tag{12}$$

where $\zeta(I) = \gamma(I) - R$ with $\gamma(I) = \frac{k\sigma I}{\tau\sigma I + 1}$. Here, k is a factor that relates received energy with growth rate and R represents the respiration rate.

2.3 Coupling of two systems

As shown in previous section, the light intensity I plays an important role in algal growth, since it triggers photosynthesis. On the other hand, the position of the algae $z(t)$ influences the light perceived as well as the efficiency of the photosynthesis process. Therefore, the light intensity is the main connection which couples the hydrodynamic model and the physiological evolution of the algae. To evaluate the light intensity observed on the trajectory z, we assume that the growth process occurs at a much slower time scale than those of hydrodynamics and is, as such, negligible for one lap over the raceway. In the same way uncertainties as rainfall and evaporation, can also be neglected at this time scale. These can be taken into account for longer time scale using more detailed models, see for instance [12, 9]. In this framework, the Beer-Lambert law describes how light is attenuated with depth:

$$I(x, z) := I_s \exp\left(-\varepsilon(\eta(x) - z)\right), \tag{13}$$

with ε the light extinction coefficient. Combining (13) with (8), we get the following expression for the captured light intensity along the trajectory z

$$I(x, z) = I_s \exp\left(-\varepsilon \frac{h(x)}{h(0)}(\eta(0) - z(0))\right).$$

In order to evaluate the quality of this coupled system, we define the average net growth rate by

$$\bar{\mu} := \frac{1}{V} \int_0^L \int_{z_b(x)}^{\eta(x)} \mu\big(C(x, z), I(x, z)\big) \mathrm{d}z \mathrm{d}x, \tag{14}$$

where μ is defined by (12) and $V := \int_0^L h(x)\mathrm{d}x$ is the volume of our 1D raceway.

3 Optimization problem

In this section, we define the optimization problem associated with our biological - hydrodynamic model. We first introduce our procedure for a simple problem, and then extend this to other variant cases.

3.1 Objective function and vertical discretization

Note that our goal is to optimize the topography of the raceway system. We choose (14) as the objective function. In order to tackle numerically this optimization problem, let us consider a vertical discretization. Let N_z denotes the number of trajectories, and consider a uniform vertical discretization of their initial position: $z_i(0) = \eta(0) - \frac{i - \frac{1}{2}}{N_z} h(0)$, $i = 1, \ldots, N_z$. From (8), we obtain $z_i(x) - z_{i+1}(x) = \frac{1}{N_z} h(x)$, $i = 1, \ldots, N_z$, meaning that the distribution of trajectories remains uniform along the trajectories. To simplify notations, we write $I_i(x)$ instead of $I(x, z_i)$ hereafter. Given $i \in \{1, \cdots, N_z\}$, let $C_i(x)$ (resp. $I_i(x)$) the photo-inhibition state (resp. the light intensity) associated with the trajectories $z_i(x)$. The semi-discrete average net growth rate in the raceway pond can be defined from (14) by

$$\bar{\mu}_{N_z} := \frac{1}{V N_z} \sum_{i=1}^{N_z} \int_0^L \mu(C_i(x), I_i(x)) h(x) \mathrm{d}x. \tag{15}$$

From now on, we focus on the subcritical case, i.e. $Fr < 1$, see Remark 2.1. As mentioned in Subsection 2.1, in this regime, a given topography z_b corresponds to a unique water depth h which verifies this assumption.

Remark 3.1. *In usual shallow water solver, equations of type (4) are usually consider to compute h in the simulations. Here, we use this equation in the opposite way, i.e., to recover the topography z_b from h.*

3.2 Periodic setting

We consider the case where the photoinhibition state C is periodic, with a period corresponding to one lap of the raceway pond. This situation occurs, e.g., when an appropriate harvest is performed after each lap. To describe the corresponding model, let us first consider a variant of the usual Cauchy problem (11): *Given $I \in \mathcal{C}(0, L; \mathbb{R}^+)$, find $(C_0, C) \in [0, 1] \times \mathcal{C}(0, L; [0, 1])$ such that*

$$\begin{cases} C'(x) = \frac{-\alpha(I(x))C(x) + \beta(I(x))}{Q_0} h(x), & x \in [0, L] \\ C(L) = C(0) = C_0. \end{cases} \tag{16}$$

Applying the Duhamel's formula on the Cauchy problem associated with (11) and the initial condition $C(0) = C_0$ and using $\beta(I) \leq \alpha(I)$, one gets successively

$$\begin{aligned} C(L) - C_0 &= - \left(1 - e^{-\int_0^L \frac{\alpha(I(s))h(s)}{Q_0} \mathrm{d}s} \right) C_0 \\ &\quad + \int_0^L e^{-\int_s^L \frac{\alpha(I(y))h(y)}{Q_0} \mathrm{d}y} \frac{\beta(I(s))h(s)}{Q_0} \mathrm{d}s \\ &\leq \left(1 - e^{-\int_0^L \frac{\alpha(I(s))h(s)}{Q_0} \mathrm{d}s} \right) (1 - C_0), \end{aligned}$$

where the equality shows that the (affine) mapping $\Phi : C_0 \mapsto C(L) - C_0$ satisfies $\Phi(0) \geq 0$, and the inequality implies that $\Phi(1) \leq 0$. It follows that there exists a unique $C_0 \in [0, 1]$ satisfying $C(L) - C_0 = 0$. This proves the next theorem.

Theorem 3.1. *There exists a unique couple* $(C_0, C) \in [0, 1] \times \mathcal{C}(0, L; [0, 1])$ *satisfying* (16).

3.3 Constant Volume

For simplicity, we omit from now on x in the notation and consider h as the variable of the intensities $(I_i)_{i=1,\ldots,N_z}$ and $\bar{\mu}_{N_z}$. Given a volume V, the optimization problem then reads:

Find $h^* \in L^\infty(0, L; \mathbb{R})$ solving the maximization problem:

$$\max_{h \in L^\infty(0,L;\mathbb{R})} \quad \bar{\mu}_{N_z}(h)$$

with the constraints

$$\begin{cases} C_i' = \dfrac{-\alpha(I_i(h))C_i + \beta(I_i(h))}{Q_0} h, \\ C_i(0) = C_i(L), \qquad \forall i = 1, \cdots, N_z, \\ v' = h, \\ v(0) = 0, \; v(L) = V. \end{cases} \tag{17}$$

The Hamiltonian associated with this optimal control problem is defined by

$$H = \sum_{i=1}^{N_z} p_i^C \left(\frac{-\alpha(I_i(h))C_i + \beta(I_i(h))}{Q_0} h \right) + p^v h - \bar{\mu}_{N_z}(h),$$

where p_i^C and p^v are the co-states of system (17). The Pontryagin Maximum Principle [7] implies that at a maximum, p_i^C and p^v satisfy

$$\begin{cases} p_i^{C\,\prime} = -\dfrac{\partial H}{\partial C_i} = p_i^C \dfrac{\alpha(I_i(h))}{Q_0} h + \dfrac{\gamma(I_i(h))}{V N_z} h, \\ p_i^C(0) = p_i^C(L), \qquad \forall i = 1, \cdots, N_z, \\ p^{v\prime} = -\dfrac{\partial H}{\partial v} = 0. \end{cases} \tag{18}$$

The last optimality condition is obtained by canceling the derivative of H with respect to h. More precisely, let $h \in L^\infty(0, L; \mathbb{R})$, and assume that $((C_i)_{i=1,\cdots,N_z}, v)$ and $((p_i^C)_{i=1,\cdots,N_z}, p^v)$ are corresponding solutions of (17),(18) respectively. Then

$$\nabla \bar{\mu}_{N_z}(h) = -\frac{\partial H}{\partial h}, \tag{19}$$

meaning that, in the case h is optimal and remains in $(0, h_c)$, then $\frac{\partial H}{\partial h} = 0$, i.e.

$$
\begin{aligned}
&\sum_{i=1}^{N_z} \frac{-\gamma'\left(I_i(h)\right) C_i + \zeta'\left(I_i(h)\right)}{V N_z} I_i'(h)h + p_i^C \frac{\alpha'(I_i(h))C_i - \beta'(I_i(h))}{Q_0} I_i'(h)h \\
&+ \sum_{i=1}^{N_z} \frac{-\gamma\left(I_i(h)\right) C_i + \zeta\left(I_i(h)\right)}{V N_z} + p_i^C \frac{\alpha(I_i(h))C_i - \beta(I_i(h))}{Q_0} + p^v = 0,
\end{aligned}
\tag{20}
$$

Theorem 3.2. *There exists $p^v \in \mathbb{R}$ such that the constant water depth $h^f := \frac{V}{L}$ and the corresponding solutions $(C_i)_{i=1,\cdots,N_z}$, $(p_i^C)_{i=1,\cdots,N_z}$ of (17), (18) respectively, satisfy the optimality condition (20).*

Proof 1. *Given $i \in \{1, \cdots, N_z\}$, from (8) and (13), we deduce that $I_i(h^f) = I_s \exp(-\varepsilon \frac{i-\frac{1}{2}}{N_z} h^f)$ and $I_i'(h^f) = -\varepsilon \frac{i-\frac{1}{2}}{N_z} I_i(h^f)$ are constant on $[0, L]$. Solving (17) gives*

$$
\begin{aligned}
C_i(x) =& e^{-\frac{\alpha(I_i(h^f))}{Q_0} h^f x} C_i(0) \\
&+ \frac{\beta(I_i(h^f))}{\alpha(I_i(h^f))}(1 - e^{-\frac{\alpha(I_i(h^f))}{Q_0} h^f x}).
\end{aligned}
\tag{21}
$$

Since C_i is periodic (i.e. $C_i(L) = C_i(0)$), we get from the previous equation that $C_i(0) = \frac{\beta(I_i(h^f))}{\alpha(I_i(h^f))}$. Inserting this value in (21), we find $C_i(x) = C_i^f := \frac{\beta(I_i(h^f))}{\alpha(I_i(h^f))}$ on $[0, L]$. A similar reasoning applied to (18) gives $p_i(x) = p_i^f = -\frac{Q_0 \gamma(I_i(h^f))}{V N_z \alpha(I_i(h^f))}$ on $[0, L]$. It follows that all the terms in the sums in (20) are constant on $[0, L]$. Hence, there exists a $p^v \in \mathbb{R}$ such that (20) is satisfied. The result follows.

Remark 3.2. *The previous theorem shows that the flat topography satisfies necessary conditions of optimality. Numerically, we observe that the flat topography is actually optimal in the periodic case (see Subsection 4.3.4).*

Remark 3.3. *If C is defined by a Cauchy problem and not assumed to be periodic, (21) implies that C may depends on x and the computations in the proof above no longer hold. In other words, the flat topography is not necessarily an optimum in a non periodic setting, which is confirmed by our numerical tests (see Subsection 4.3.2).*

3.4 Non-constant volume problem for maximizing areal productivity

In general, the volume of the system can also change hence can be optimized. In this way, we now assume that the water depth is of the form $h + h_0$, where $h_0 \in \mathbb{R}^+$ and $h \in L^\infty(0, L; \mathbb{R})$ with $\int_0^L h = 0$, so that $V = h_0 L$. On the other hand, the biomass concentration X (defined by $\dot{X} = (\bar{\mu} - D)X$ with D dilution rate) changes with the system volume V, meaning that the light extinction ε in (13) can no longer be assumed to be constant. Hence, we consider that

$\varepsilon(X) := \varepsilon_0 X + \varepsilon_1$, where $\varepsilon_0 > 0$ is the specific light extinction coefficient of the microalgae species and ε_1 the background turbidity that summarizes the light absorption and diffusion caused by all non-microalgae components [22]. A standard criterion to determine a relevant value of X (see [23, 17]) consists in regulating it such that the steady state value of the net growth rate μ at the average depth h_0 is 0, i.e.,

$$\mu_0(I(h_0)) = 0, \qquad (22)$$

where μ_0 is defined by $\mu_0(I) := -\gamma(I)\frac{\beta(I)}{\alpha(I)} + \zeta(I)$. This condition is equivalent to the fact that $I(h_0)$ is one of the two roots (I_-, I_+) of the second order polynomial function $I \mapsto k_d\tau R(\sigma I)^2 + (k_r\tau\sigma R - k_r k\sigma)I + k_r R = 0$. In practice (I_-, I_+) are real, $I_- \leq I_+$ and X is adjusted to get $I(h_0) = I_-$. We refer to [2] for the corresponding analysis. Note that $\mu_0(I) \geq 0$ on (I_-, I_+). Assumption (22) is usually called the *compensation condition*, and describes a situation where the growth at the bottom compensates exactly the respiration. In this framework, maximizing areal productivity is a relevant target. For a given biomass concentration X, this one is given by $\Pi := \bar{\mu} X \frac{V}{S}$, where $\bar{\mu}$ is defined in (14) and S is the ground surface of the raceway pond; in our 1D system $S = L$. The total biomass X in a given volume is maintained constant to achieve the compensation conditions (22). Using (13) with $I(x, z) = I_-$, we get $X(h_0) = \frac{Y_{\mathrm{opt}}/h_0 - \varepsilon_1}{\varepsilon_0}$, with $Y_{\mathrm{opt}} := \ln(\frac{I_s}{I_-})$. We then consider the problem:

Find $(h^*, h_0^*) \in L^\infty(0, L; \mathbb{R}) \times \mathbb{R}^+$ solving the maximization problem:

$$\max_{h \in L^\infty(0,L;\mathbb{R}), h_0 \in \mathbb{R}^+} \Pi(h, h_0)$$

where $\Pi(h, h_0) := \bar{\mu}_{N_z}(h + h_0)X(h_0)h_0$, with the constraints

$$\begin{cases} C_i' = \dfrac{-\alpha(I_i(h + h_0))C_i + \beta(I_i(h + h_0))}{Q_0}(h + h_0), \\ C_i(0) = C_i(L), \qquad \forall i = 1, \cdots, N_z, \\ v' = h, \\ v(0) = 0, \ v(L) = 0. \end{cases} \qquad (23)$$

The associated Hamiltonian reads

$$\widetilde{H} = \sum_{i=1}^{N_z} p_i^C \left(\frac{-\alpha(I_i(h + h_0))C_i + \beta(I_i(h + h_0))}{Q_0}(h + h_0) \right)$$
$$+ p^v h - \bar{\mu}_{N_z}(h + h_0)X(h_0)h_0.$$

Analysis similar to that in Subsection 3.1 gives

$$\nabla\Pi(h, h_0) = (-\frac{\partial \widetilde{H}}{\partial h}, -\frac{\partial \widetilde{H}}{\partial h_0}), \qquad (24)$$

in which $((C_i)_{i=1,\cdots,N_z}, v)$ satisfies (23), $((p_i^C)_{i=1,\cdots,N_z}, p^v)$ satisfies (18) and where h and $\gamma(\cdot)$ are replaced by $h + h_0$ and $X(h_0)h_0\gamma(\cdot)$ respectively. Unlike Theorem 3.2, the flat topography does not cancel $\nabla\Pi$.

11

Theorem 3.3. *Let $h_0 > 0$ and assume that $\mu(I_s) > 0$ (or, equivalently $I_s \in (I_-, I_+)$). Then $\nabla\Pi(0, h_0) \neq 0$.*

Proof 2. *First, note that differentiating $I_i(h + h_0) = I_s \exp\left(-\frac{Y_{opt}}{h_0}\frac{i - \frac{1}{2}}{N_z}(h + h_0)\right)$ with respect to h_0 and setting $h = 0$, we get $\partial_{h_0} I_i(h_0 + h)|_{h=0} = 0$. Then, analysis similar to that in the proof of Theorem 3.2 shows that C_i is constant as soon as $h = 0$, so that $-\alpha(I_i(h_0))C_i + \beta(I_i(h_0)) = 0$. Using these two properties, we get $\frac{\partial\widetilde{H}}{\partial h_0} = \frac{\varepsilon_1}{N_z \varepsilon_0}\sum_{i=1}^{N_z}\mu_0(I_i(h_0))$. Since $I_i(h_0) \in [I_{N_z}(h_0), I_1(h_0)] \subset (I_-, I_s) \subset (I_-, I_+)$, we get $\mu_0(I_i(h_0)) > 0$ for $i \in \{1, \cdots, N_z\}$. The result follows.*

Remark 3.4. *Note that the coefficient h_0 considered in Theorem 3.3 needs to satisfy $h_c \leq h_0$ to guarantee that the system remains in a subcritical regime (see Remark 2.1).*

4 Numerical Experiments

In this section, we show some optimal topographies obtained in the various previous frameworks.

4.1 Numerical Methods

To solve our optimization problem numerically, we introduce a supplementary space discretization with respect to x. In this way, let us take a space increment Δx, set $N_x = [L/\Delta x]$ and $x^{n_x} = n_x \Delta x$ for $n_x = 0, \ldots, N_x$. We choose to use the Heun's method for computing $(C_i)_{i=1}^{N_z}$ via (17). Following a first-discretize-then-optimize strategy, we get that the costate $(p_i^C)_{i=1}^{N_z}$ are also computed by a Heun's type scheme. Note that this scheme is still explicit since it solves a backward dynamics starting from $p_i(L) = 0$. The optimization is then achieved by a standard gradient method using (19) and (24), where the stopping criterion involves both the magnitude of the gradient and the constraint $h \geq h_c$, see Remark 2.1.

4.2 Parameter settings

We now detail the parameters used in our simulations.

4.2.1 Parameterization of h

We choose to parameterize h by a truncated Fourier series in our numerical tests. More precisely, h reads:

$$h(x) = h_0 + \sum_{i=1}^{N} a_i \sin(2n\pi\frac{x}{L}).$$

This parameterization is motivated by three reasons.

- The regularity of the topography is controlled by the order of truncation N. As an example, limit situations where $N \to +\infty$ are not considered in what follows. This framework is consistent with the hydrodynamic regime under consideration, where the solutions of the Saint-Venant equations are smooth.

- Using this parameterization, one has automatically $h(0) = h(L)$, which fits with the toric shape of the raceway pond.

- Using this parameterization, h depends in an affine way on h_0, as assumed in Section 3.4.

From (2) and (4), the velocity u and the topography z_b read also as functions of a. Once we find the vector a maximizing the functional $\bar{\mu}_{N_z}$, we then find the optimal topography of our system.

4.2.2 Parameter for the models

The spatial increment is set to $\Delta x = 0.01\,\mathrm{m}$ so that the convergence of the numerical scheme has been ensured, and we set the raceway length $L = 100\,\mathrm{m}$, the averaged discharge $Q_0 = 0.04\,\mathrm{m}^2\,\mathrm{s}^{-1}$, the average depth (in constant volume case) $h_0(= h(0; a)) = 0.4\,\mathrm{m}$ and $z_b(0) = -0.4\,\mathrm{m}$ to stay in standard ranges for a raceway. The free-fall acceleration $g = 9.81\,\mathrm{m\,s}^{-2}$. All the numerical parameters values for Han's model are taken from [16] and given in Table 1.

Table 1: Parameter values for Han Model

k_r	$6.8\ 10^{-3}$	s^{-1}
k_d	$2.99\ 10^{-4}$	-
τ	0.25	s
σ_H	0.047	$\mathrm{m}^2\,\mu\mathrm{mol}^{-1}$
k_H	$8.7\ 10^{-6}$	-
R	$1.389\ 10^{-7}$	s^{-1}

In order to determinate the light extinction ε, two cases must be considered, namely:

- constant volume: we assume that only 1% of light can be captured by the cells at the average depth of the raceway, meaning that $I_- = 0.01 I_s$, we choose $I_s = 2000\,\mu\mathrm{mol\,m}^{-2}\,\mathrm{s}^{-1}$ which approximates the maximum light intensity, e.g., at summer in the south of France. Then ε can be computed by $\varepsilon = (1/h_0)\ln(I_s/I_-)$.

- non-constant volume: in the case, h_0 is also a parameter to be optimized. We take from [22] the specific light extinction coefficient of the microalgae specie $\varepsilon_0 = 0.2\,\mathrm{m}^2 \cdot \mathrm{g}$ and the background turbidity $\varepsilon_1 = 10\,\mathrm{m}^{-1}$.

13

4.3 Numerical results

We test the influence of various parameters on optimal topography. In all our experiments, we always observe that the topographies satisfy $\min_{x \in [0,L]} h(x;a) > h_c$.

4.3.1 Influence of vertical discretization

The first test consists in studying the influence of the vertical discretization parameter N_z. We choose $N = 5$, $C_0 = 0.1$ and consider 100 random values a. Note that the choice of a should respect the subcritical condition. Let N_z varies from 1 to 80, and we compute the average value of $\bar{\mu}_{N_z}$ for each N_z. The results are shown in Fig. 3. We observe numerical convergence when N_z grows,
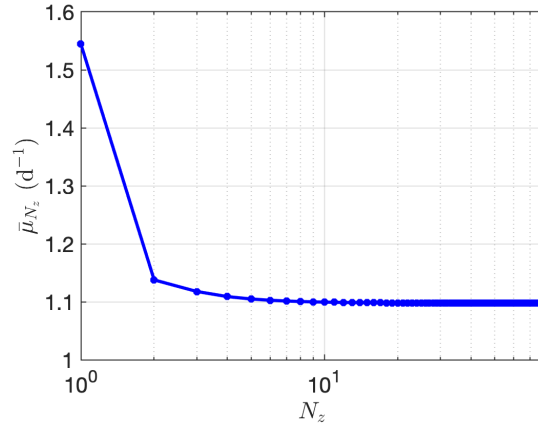

Figure 3: The value of the functional $\bar{\mu}_{N_z}$ for $N_z = [1, 80]$.

showing the convergence towards the model continuous in space. In view of these results, we take hereafter $N_z = 40$.

4.3.2 Influence of the initial condition

Here we study the influence of the initial condition C_0 on the optimal shape of the raceway pond. We set the numerical tolerance to Tol= 10^{-10}, and consider the order of truncation $N = 5$. As for the initial guess, we consider the flat topography, meaning that a is set to 0. We compare the optimal topographies obtained with $C_0 = 0.1$ and with $C_0 = 0.9$. The result is shown in Fig. 4. This test confirms Remark 3.3, since we obtain non-trivial topographies which slightly enhance the algal average growth rate. Moreover, a slight difference between the two optimal topographies is observed. We have observed that this difference remains when the spatial increment Δx goes to zero.
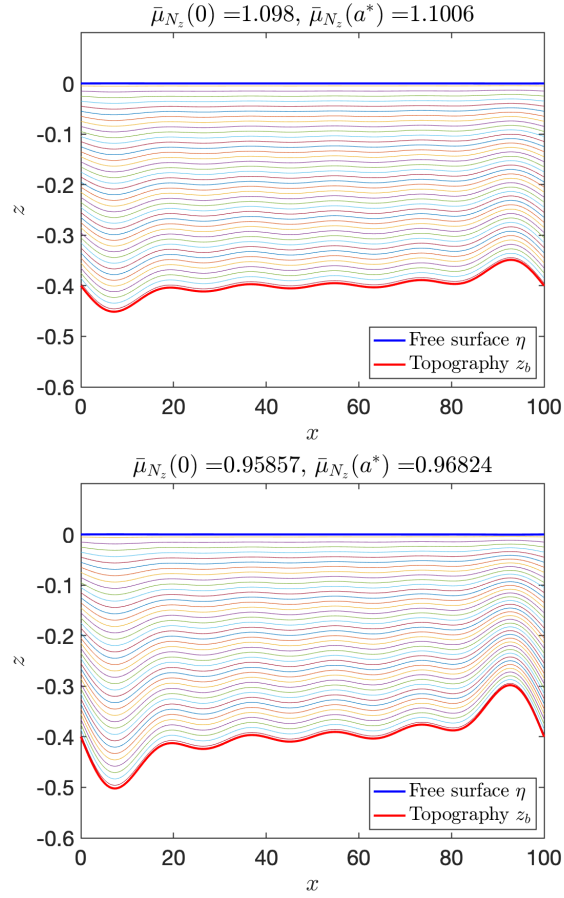
Figure 4: The optimal topography for $C_0 = 0.1$ (Top) and $C_0 = 0.9$ (Bottom). The red thick line represents the topography z_b, the blue thick line represents the free surface η, and all the other curves between represent the different trajectories. $\bar{\mu}_{N_z}(0)$: flat topography, $\bar{\mu}_{N_z}(a^*)$: optimal topography.

4.3.3 Influence of Fourier series truncation

The next test is dedicated to study the influence of the order of truncation N used to parameterize the water depth h. Set $N = [0, 5, 10, 15, 20]$, $C_0 = 0.1$ and keep all the other parameters as in the previous section. Table 2 shows the optimal value of the objective function $\bar{\mu}_{N_z}(a^*)$ for different orders of truncation N. The result shows a slight increase in the optimal value of the objective

Table 2: The objective function for different orders of truncation N.

N	Iter	$\bar{\mu}_{N_z}(a^*)(\mathrm{d}^{-1})$	$\log_{10}(\|\nabla\bar{\mu}_{N_z}(a^*)\|)$
0	0	1.098	$-$
5	16	1.1006	-10.208017
10	17	1.1013	-10.240885
15	17	1.1016	-10.258798
20	18	1.1018	-10.269413

function $\bar{\mu}_{N_z}(a^*)$ when N becomes larger. However, the corresponding values of $\bar{\mu}_{N_z}(a^*)$ remain close to the one associated with a flat topography.

4.3.4 Optimal topographies in periodic case

We study the optimal topographies in the case where the photoinhibition state C is periodic. In the constant volume case, we observe that the optimization procedure always converges to a flat topography (i.e. $a^* = a_f$) for random admissible initial guesses a. This leads us to conjecture that the flat topography corresponds to the global maximum for the average growth rate. As for the variable volume case, let us set $N = 5$ (i.e. $\tilde{a} \in \mathbb{R}^6$) and $h_0 = 0.4$ as initial guess of average depth. We observe that the optimization stops due to the presence of the physical constraint h_c. However, a smaller depth boosts the areal productivity which in some cases can increase for more than twice with respect to the initial areal productivity.

4.3.5 Simulation with paddle wheel

In this paragraph we consider the full raceway pond, where the mixing induced by the paddle wheel is also considered. More precisely, we simulate several laps with a paddle wheel that mixes up the algae after each lap. The turbulent mixing of the paddle wheel is modelled by a permutation matrix P which rearranges the trajectories at each lap. In our test, P is chosen as an anti-diagonal matrix with the entries one. This choice actually corresponds to an optimum and as shown in [5], where other choices are also investigated.

The permutation matrix P corresponds to the permutation $\pi = (1N_z)(2N_z - 1)(3N_z - 2)\ldots$, where we use the standard notation of cycles in the symmetric group. Note that π is of order two. The photoinhibition state C is then set

to be 2-periodic (i.e $C^1(0) = PC^2(L)$, where C^1 and C^2 corresponds to the photoinhibition state during the first and the second lap, respectively). The details of the optimization procedure are given in Appendix A.

We choose a truncation of order $N = 5$ in the Fourier series. The initial guess a set to be zero. Fig. 5 presents the shape of the optimal topography and the evolution of the photoinhibition state C over two laps. The resulting optimal
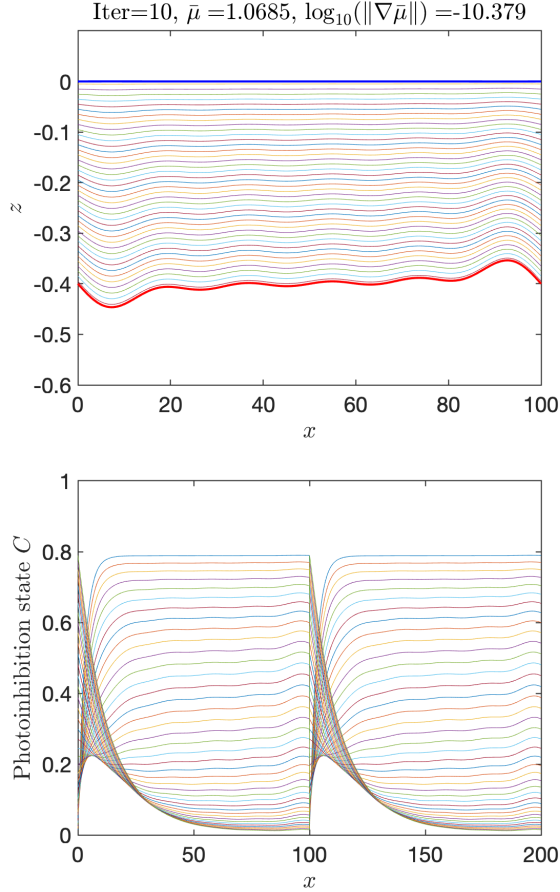

Figure 5: The optimal topography (Top) and the evolution of the photo-inhibition state C (Bottom) for two laps.

topography in this case is not flat. However, the increase in the optimal value of the objective function $\bar{\mu}_{N_z}$ compares to a flat topography is around 0.217%, and compares to a flat topography and non permutation case is around 0.265%, in both cases, the increase remains small. On the other hand, we observe that the state C is actually periodic for each lap. This result is actually proved for arbitrary P in [5] in the case of a flat topography. This justifies that the optimization strategy only need to focus on one lap of the raceway (whatever

17

the permutation), and leaves the door open to the optimization of such mixing strategies. We refer to [3, 4] for further details about optimal mixing strategies.

5 Conclusions and future works

A flat topography cancels the gradient of average algal growth rate when C is assumed to be periodic along the laminar parts of the raceway. This is further confirmed by our numerical tests where maximum productivity is obtained for a flat topography. However, considering a more complete framework without periodicity and including a mixing device gives rise to an optimal non flat topography with a slight gain of the average growth rate. It is not clear if the difficulty to design such a pattern could be compensated by the increase in the process productivity.

These results may not hold anymore if the hydrodynamic regime is turbulent along the entire raceway. In such a case, the increase in algal productivity may compensate the higher energetic cost to mix the raceway. However, without the laminar assumption, the problem becomes challenging, and much work remains to be done in this direction.

References

[1] O. Bernard, A.-C. Boulanger, M.-O. Bristeau, and J. Sainte-Marie. A 2d model for hydrodynamics and biology coupling applied to algae growth simulations. *ESAIM: Mathematical Modelling and Numerical Analysis*, 47(5):1387–1412, September 2013.

[2] O. Bernard and L.-D. Lu. Optimal optical conditions for microalgal production in photobioreactors, 2021. To appear in Journal of Process Control.

[3] O. Bernard, L.-D. Lu, and J. Salomon. Mixing strategies combined with shape design to enhance productivity of a raceway pond. In *16th IFAC Symposium on Advanced Control of Chemical Processes ADCHEM 2021*, volume 54, pages 281–286, 2021.

[4] O. Bernard, L.-D. Lu, and J. Salomon. Optimization of mixing strategy in microalgal raceway ponds. Submitted, 2021.

[5] O. Bernard, L.-D. Lu, and J. Salomon. Optimizing microalgal productivity in raceway ponds through a controlled mixing device. In *2021 American Control Conference (ACC)*, pages 640–645. IEEE, 2021.

[6] O. Bernard, F. Mairet, and B. Chachuat. Modelling of microalgae culture systems with applications to control and optimization. *Microalgae Biotechnology*, 153(59-87), 2015.

[7] V. G. Boltyanskiy, R. V. Gamkrelidze, Y. E. F. Mishchenko, and L. S. Pontryagin. *Mathematical theory of optimal processes*. Routledge, 1962.

[8] A. Bouharguane and B. Mohammadi. Minimization principles for the evolution of a soft sea bed interacting with a shallow. *International Journal of Computational Fluid Dynamics*, 26(3):163–172, May 2012.

[9] F. Casagli, G. Zuccaro, O. Bernard, J.-P. Steyer, and E. Ficara. Alba: A comprehensive growth model to optimize algae-bacteria wastewater treatment in raceway ponds. *Water Research*, 190:116734, 2021.

[10] D. Chiaramonti, M. Prussi, D. Casini, M.R. Tredici, L. Rodolfi, N. Bassi, G.C. Zittelli, and P. Bondioli. Review of energy balance in raceway ponds for microalgae cultivation: Re-thinking a traditional system is possible. *Applied Energy*, 102:101–111, Feburary 2013.

[11] P.-H. Cocquet, S. Riffo, and J. Salomon. Optimization of bathymetry for long waves with small amplitude. *SIAM Journal on Control and Optimization*, 59(6):4429–4456, 2021.

[12] R. De-Luca, F. Bezzo, Q. Béchet, and O. Bernard. Exploiting meteorological forecasts for the optimal operation of algal ponds. *Journal of Process Control*, 55:55–65, 2017.

[13] D. Demory, C. Combe, P. Hartmann, A. Talec, E. Pruvost, R. Hamouda, F. Souillé, P.-O. Lamare, M.-O. Bristeau, J. Sainte-Marie, S. Rabouille, F. Mairet, A. Sciandra, and O. Bernard. How do microalgae perceive light in a high-rate pond? towards more realistic lagrangian experiments. *The Royal Society*, May 2018.

[14] P.H.C. Eilers and J.C.H. Peeters. Dynamic behaviour of a model for photosynthesis and photoinhibition. *Ecological Modelling*, 69(1):113 – 133, 1993.

[15] J.-F. Gerbeau and B. Perthame. Derivation of viscous saint-venant system for laminar shallow water; numerical validation. *Discrete & Continuous Dynamical Systems - B*, 1(1):89–102, Feburary 2001.

[16] J. Grenier, F. Lopes, H. Bonnefond, and O. Bernard. Worldwide perspectives of rotating algal biofilm up-scaling. Submitted, 2020.

[17] F. Grognard, A.R. Akhmetzhanov, and O. Bernard. Optimal strategies for biomass productivity maximization in a photobioreactor using natural light. *Automatica*, 50(2):359–368, 2014.

[18] B.-P. Han. A mechanistic model of algal photoinhibition induced by photodamage to photosystem-ii. *Journal of theoretical biology*, 214(4):519–527, February 2002.

[19] R. Hreiz, B. Sialve, J. Morchain, R. Escudié, J.-P. Steyer, and P. Guiraud. Experimental and numerical investigation of hydrodynamics in raceway reactors used for algaculture. *Chemical Engineering Journal*, 250:230–239, 2014.

[20] C. Inostroza, A. Solimeno, J. García, J.M. Fernández-Sevilla, and F.G. Acién. Improvement of real-scale raceway bioreactors for microalgae production using computational fluid dynamics (cfd). *Algal Research*, 54:102207, 2021.

[21] P.-O. Lamare, N. Aguillon, J. Sainte-Marie, J. Grenier, H. Bonnefond, and O. Bernard. Gradient-based optimization of a rotating algal biofilm process. *Automatica*, 105:80–88, July 2019.

[22] C. Martínez, F. Mairet, and O. Bernard. Theory of turbid microalgae cultures. *Journal of Theoretical Biology*, 456:190–200, November 2018.

[23] P. Masci, F. Grognard, and O. Bernard. Microalgal biomass surface productivity optimization based on a photobioreactor model. *IFAC Proceedings Volumes*, 43(6):180–185, 2010.

[24] J. Masojídek, Š. Papáček, M. Sergejevová, V. Jirka, J. Červený, J. Kunc, J. Korečko, O. Verbovikova, J. Kopecký, D. Štys, and G. Torzillo. A closed solar photobioreactor for cultivation of microalgae under supra-high irradiance: Basic design and performance. *Journal of Applied Phycology*, 15(2-3):239–248, 2003.

[25] J.L. Mendoza, M.R. Granados, I. De Godos, F.G. Acién, E. Molina, C. Banks, and S. Heaven. Fluid-dynamic characterization of real-scale raceway reactors for microalgae production. *Biomass and Bioenergy*, 54:267–275, 2013.

[26] V. Michel-Dansac, C. Berthon, S. Clain, and F. Foucher. A well-balanced scheme for the shallow-water equations with topography. *Computers and Mathematics with Applications*, 72(3):586–593, August 2016.

[27] B. Mohammadi and A. Bouharguane. Optimal dynamics of soft shapes in shallow waters. *Computers and Fluids*, 40(1):291–298, January 2011.

[28] R. Muñoz-Tamayo, F. Mairet, and O. Bernard. Optimizing microalgal production in raceway systems. *Biotechnology progress*, 29(2):543–552, 2013.

[29] G. Olivieri, L. Gargiulo, P. Lettieri, L. Mazzei, P. Salatino, and A. Marzocchella. Photobioreactors for microalgal cultures: A lagrangian model coupling hydrodynamics and kinetics. *Biotechnology progress*, 31(5):1259–1272, 2015.

[30] S. Papacek, J. Jablonsky, and K. Petera. Advanced integration of fluid dynamics and photosynthetic reaction kinetics for microalgae culture systems. *BMC systems biology*, 12(5):1–12, 2018.

[31] C. Posten and S.F. Chen, editors. *Microalgae Biotechnology.* 153. Springer, 1 edition, 2016.

[32] M. Prussi, M. Buffi, D. Casini, D. Chiaramonti, F. Martelli, M. Carnevale, M.R. Tredici, and L. Rodolfi. Experimental and numerical investigations of mixing in raceway ponds for algae cultivation. *Biomass and bioenergy*, 67:390–400, 2014.

[33] A. van Dongeren, N. Plant, A. Cohen, D. Roelvink, M.C. Haller, and P. Catalán. Beach wizard: Nearshore bathymetry estimation through assimilation of model computations and remote observations. *Coastal Engineering*, 55(12):1016–1027, December 2008.

[34] R.H. Wijffels and M.J. Barbosa. An outlook on microalgal biofuels. *Science*, 329(5993):796–799, August 2010.

[35] S.J. Yoo, S.-K. Oh, and J.M. Lee. Design of experiments and sensitivity analysis for microalgal bioreactor systems. In Ian David Lockhart Bogle and Michael Fairweather, editors, *22nd European Symposium on Computer Aided Process Engineering*, volume 30 of *Computer Aided Chemical Engineering*, pages 722 – 726. Elsevier, 2012.

A   System with a paddle-wheel

Let us denote by P the permutation matrix associated with π, i.e., 1 as entries on the anti-diagonal. Let us denote by C^1 (resp. C^2) the photoinhibition state for the first (resp. second) lap of the raceway. We then assume that the state C is 2-periodic, meaning that $C^1(0) = PC^2(L)$. From (15), we define the objective function by $\frac{1}{2} \sum_{j=1}^{2} \bar{\mu}_{N_z}^j(h) = \frac{1}{2VN_z} \sum_{j=1}^{2} \sum_{i=1}^{N_z} \int_0^L \frac{-\gamma(I_i(h))C_i^j + \zeta(I_i(h))}{Q_0} h \mathrm{d}x$. Given a volume V, the optimization problem reads:

Find $h^* \in L^\infty(0, L; \mathbb{R})$ solving the maximization problem:

$$\max_{h \in L^\infty(0,L;\mathbb{R})} \quad \frac{1}{2} \sum_{j=1}^{2} \bar{\mu}_{N_z}(h)$$

with the constraints

$$\begin{cases} C_i^{j\prime} = \dfrac{-\alpha(I_i(h))C_i^j + \beta(I_i(h))}{Q_0} h, \\ C^1(L) = PC^2(0), \\ C^1(0) = PC^2(L), \\ \quad v' = h, \\ \quad v(0) = 0, \ v(L) = V. \end{cases} \tag{25}$$

Let us still denote by H the Hamiltonian associated with this optimization problem. It can then be written

$$H = \sum_{j=1}^{2} \sum_{i=1}^{N_z} p_i^{C^j} \left(\frac{-\alpha(I_i(h))C_i^j + \beta(I_i(h))}{Q_0} h \right) + p^v h - \frac{1}{2} \sum_{j=1}^{2} \bar{\mu}_{N_z}^j(h),$$

where $p_i^{C^j}$ and p^v are the co-states of system (25). Analysis similar to that in Subsection 3.1 gives $\nabla \left(\frac{1}{2} \sum_{j=1}^{2} \bar{\mu}_{N_z}^{j}(h) \right) = -\dfrac{\partial H}{\partial h}$, in which $p_i^{C^j}$ and p^v satisfy (18) with $p^{C^1}(L) = P p^{C^2}(0)$ and $p^{C^2}(L) = P p^{C^1}(0)$.